

Surface features, rotation and atmospheric variability of ultra cool dwarfs

C.A.L. Bailer-Jones

Max-Planck-Institut für Astronomie, Königstuhl 17, D-69117 Heidelberg, Germany
 email: calj@mpia-hd.mpg.de

Abstract. Photometric I band light curves of 21 ultra cool M and L dwarfs are presented. Variability with amplitudes of 0.01 to 0.055 magnitudes (RMS) with typical timescales of an hour to several hours are discovered in half of these objects. Periodic variability is discovered in a few cases, but interestingly several variable objects show no significant periods, even though the observations were almost certainly sensitive to the expected rotation periods. It is argued that in these cases the variability is due to the evolution of the surface features on timescales of a few hours. This is supported in the case of 2M1145 for which no common period is found in two separate light curves. It is speculated that these features are photospheric dust clouds, with their evolution possibly driven by rotation and turbulence. An alternative possibility is magnetically-induced surface features. However, chromospheric activity undergoes a sharp decrease between M7 and L1, whereas a greater occurrence of variability is observed in objects later than M9, lending support to the dust interpretation.

Keywords: light curves – variability – rotation – dust clouds

To appear in *Ultracool Dwarf Stars* (Lecture Notes in Physics), H.R.A. Jones, I. Steele (eds), Springer-Verlag, 2001

1 Introduction

Large numbers of very cool compact objects – namely low mass stars, brown dwarfs and giant gas planets – have only recently become available through large scale surveys, particularly in the far red and near infrared where these objects radiate most of their energy. This has presented the opportunity to systematically study their intrinsic properties. Indeed, the L dwarf sequence has recently been introduced to account for the increasing number of objects found with effective temperatures apparently in the range 2200–1300 K [04][14][15][21], and the T dwarf class covers the even cooler objects (similar to Gl 229B) now being discovered [06][17][23].

For a number of reasons, these ultra cool dwarfs are likely to have interesting and complex atmospheres. First, they are fully convective. Second, many are rapid rotators [04]. Third, at these low temperatures, solid dust particles, or condensates, form. These first two properties may be a driver for atmospheric dynamics, or weather, and the presence of dust makes it possible that large-scale clouds form. Although these objects cannot (yet) be resolved, the presence of weather patterns can be investigated by via accurate photometric monitoring, which is the subject of this article.

1.1 Previous Work

Initial attempts to observe variability in ultra cool dwarfs have met with mixed results. Terndrup et al. [28] searched for rotational modulation of the light curves of eight M-type stars and brown dwarfs in the Pleiades. They derived periodicities for two low mass stars, but found no significant variability in the rest of the sample. Tinney & Tolley [29] found some evidence for variability in an M9 brown dwarf with an amplitude of 0.04 magnitudes over a few hours, but detected no variability above 0.1 magnitudes in an L5 dwarf. Nakajima et al. [22] found variability in the near infrared spectrum of a T dwarf over a period of 80 minutes. In a precursor to the present project, Bailer-Jones & Mundt [01] observed six M and L dwarfs and found variability in one (2M1145), to which a tentative period of 7.1 hours was assigned (pending confirmation).

1.2 Observational Sample

This paper reports results from an observational program to monitor photometric I band variability in a sample of 21 late M and L dwarfs (Table 1). Only about 30 L dwarfs were known at the time of the observations, thus greatly limiting the choice of targets. Objects brighter than $I = 19.0$ were preferentially selected, but there are no other (known) selection biases. Ten of the targets are field dwarfs discovered by the Two Micron All Sky Survey (2MASS) and the Sloan Digital Sky Survey (SDSS). Five objects are members of the Pleiades (age 120 Myr): Teide 1 and Calar 3 are confirmed brown dwarfs, Roque 11 and 12 are probably brown dwarfs, and Roque 16 is very close to the hydrogen burning limit (so its status is uncertain). The six remaining objects are candidate members of the σ Orionis cluster (age 1–5 Myr), with masses between 0.02 and $0.12 M_{\odot}$.

2 Observations and Data Reduction

The targets were observed with a CCD camera on the 2.2m telescope at the Calar Alto Observatory (Spain) over three periods: January 1999 (AJD 1187.4–1192.8, hereafter 99-01), September 1999 (AJD 1432.8–1436.2, hereafter 99-09) and February 2000 (AJD 1601.8–1607.2, hereafter 00-02). AJD=JD-2450000. Exposure times of 8 minutes were used for most objects to achieve a signal-to-noise ratio (SNR) for the target objects of at least 100. Objects were observed repeatedly each night for several nights to construct a light curve with typically 30 points. The data reduction consisted of careful flat fielding and fringe removal to reduce all errors to less than 0.5%. More details are given in Bailer-Jones & Mundt [02].

3 Light Curve Analysis: Theory

Differential light curves were obtained for each target relative to a number of reference stars in the field. These reference stars were chosen to be bright and

Table 1. Properties of the ultra cool dwarf targets. Each reference makes use of a different I band and even definition of magnitude, so values are only intended to be indicative. In particular, the SDSS I filter is somewhat bluer than the Cousins I filter, thus yielding fainter magnitudes for L dwarfs. The spectral types in parentheses have been estimated from the $R - I$ colours in [05].

name	IAU name	I	SpT	$H\alpha$ EW Å	LiI EW Å	ref
2M0030	2MASSW J0030438+313932	18.82	L2	4.4 ± 0.2	< 1.0	[14]
2M0326	2MASSW J0326137+295015	19.17	L3.5	9.1 ± 0.2	< 1.0	[14]
2M0345	2MASSW J0345432+254023	16.98	L0	≤ 0.3	< 0.5	[14]
2M0913	2MASSW J0913032+184150	19.07	L3	< 0.8	< 1.0	[14]
2M1145	2MASSW J1145572+231730	18.62	L1.5	4.2 ± 0.2	< 0.4	[14]
2M1146	2MASSW J1146345+223053	17.62	L3	≤ 0.3	5.1 ± 0.2	[14]
2M1334	2MASSW J1334062+194034	18.76	L1.5	4.2 ± 0.2	< 1.5	[14]
2M1439	2MASSW J1439284+192915	16.02	L1	1.13 ± 0.05	< 0.05	[25]
SDSS 0539	SDSSp J053951.99-005902.0	19.04	L5			[11]
SDSS 1203	SDSSp J120358.19+001550.3	18.88	L3			[11]
Calar 3		18.73	M9	$6.5 - 10.2$	1.8 ± 0.4	[26]
Roque 11	RPL J034712+2428.5	18.75	M8	5.8 ± 1.0		[30]
Roque 12		18.47	M7.5	19.7 ± 0.3	≤ 1.5	[20]
Roque 16	RPL J034739+2436.4	17.79	M6	5.0 ± 1.0		[30]
Teide 1	TPL J034718+2422.5	18.80	M8	$3.5 - 8.6$	1.0 ± 0.2	[24]
S Ori 31	S Ori J053820.8-024613	17.31	(M6.5)			[05]
S Ori 33	S Ori J053657.9-023522	17.38	(M6.5)			[05]
S Ori 34	S Ori J053707.1-023246	17.46	(M6)	≤ 5.0		[05]
S Ori 44	S Ori J053807.0-024321	19.39	M6.5	60.0 ± 1.0		[05]
S Ori 45	S Ori J053825.5-024836	19.59	M8.5			[05]
S Ori 46	S Ori J053651.7-023254	19.82	(M8.5)			[05]

isolated. Fluxes for all objects and reference stars were determined using aperture photometry with an aperture radius of 3.5 pixels ($1.9''$). The average flux of the reference stars forms a magnitude against which fluctuations in the target are monitored. The zero-mean differential light curve for each target, consisting of K points (or epochs), is denoted $m_d(1), m_d(2), \dots, m_d(k), \dots, m_d(K)$. The *total* photometric error at each point, $\delta m_d(k)$, has been carefully determined considering photon-noise statistics plus contributions from imperfect flat fielding and fringe correction.

3.1 χ^2 Test and Reference Star Rejection

A general test of variability is made using a χ^2 test, in which we evaluate the probability, p , that the deviations in the light curve are consistent with the photometric errors. The statistic is

$$\chi^2 = \sum_k^K \left(\frac{m_d(k)}{\delta m_d(k)} \right)^2 \quad (1)$$

such that a large χ^2 indicates greater deviation compared to the errors, and thus a smaller p . An object is considered variable if $p < 0.01$ (a 99% confidence level).

This test is first used to iteratively remove variable reference stars, by calculating the light curve for each reference star relative to all the other reference stars. The most variable reference star is removed from the reference list, and the procedure repeated until only non-variable reference stars remain (i.e. those with $p > 0.01$). Due to the large number of reference stars used (typically 20–30), any residual low-level variability in any one object will be greatly reduced in the averaged reference level.

The reliability of the χ^2 test depends on an accurate determination of the magnitude errors in the target. This has been confirmed, as objects of similar brightness to the target have variations no larger than the photometric errors for the target, thus ensuring that the errors have not been overestimated.

3.2 Power Spectrum Analysis

Evidence for *periodic* variability was searched for using the *power spectrum* or periodogram. A dominant periodicity may be present at the rotation period due to rotational modulation of the light curve by surface inhomogeneities. The power spectrum of a continuous light curve, $g(t)$, is $|G(\nu)|^2$, where $G(\nu) = \text{FT}[g]$ and FT denotes a Fourier transform. However, the target objects are only observed at the discrete time intervals given by the sampling function, $s(t)$. Thus the power spectrum of the measured *discrete* light curve, $d(t) = g(t)s(t)$, is $|D(\nu)|^2$, where $D(\nu) = \text{FT}[d(t)] = G(\nu) \otimes W(\nu)$. $W(\nu) = \text{FT}[s(t)]$ is the *spectral window function* and \otimes is the convolution operator. Thus the measured power spectrum, $|D(\nu)|^2$, may show spurious features due to the way in which the true continuous light curve was sampled. Such features are not intrinsic to the source and may obscure features which are [10][27], particularly at the low SNRs considered here.

However, it is possible to estimate $G(\nu)$ (power and phases) from the raw or *dirty* power spectrum through an iterative deconvolution using the CLEAN algorithm, which was first introduced to reconstruct aperture synthesis data in radio astronomy [27]. The resulting *cleaned* spectrum generally consists of peaks at a number of distinct frequencies, plus a residual spectrum and noise. The CLEAN code used calculates the power and phases of the components in the window function and the cleaned power spectrum [18]. The noise in the power spectrum is calculated from the photometric errors and the time sampling, and is stated in the captions to the power spectra in the next section. Peaks which are not more than several times this noise level should not be considered significant. The uncertainty in a determined frequency in the power spectrum is set by t_{max} , and is approximately $\tau^2/(2t_{\text{max}})$ for a period τ . However, for very short periods the error is constant due to the finite integration time. The longest period to which the observations are sensitive is of order t_{max} .

4 Results

4.1 General Results

The results of the application of the χ^2 test to the 21 targets are shown in Table 2 for the detections and Table 3 for the non-detections of variability. For those objects in which we did not detect variability, we have set upper limits on the amplitude. This was done by creating a set of synthetic light curves by multiplying each $m_d(k)$ by $1 + a$, for increasing (small) values of a . The amplitude limits were obtained from that synthetic light curve which gave $p = 0.01$ according to the χ^2 test. Note that a number of detections are close to the confidence limit of $p = 0.01$, so the division between Tables 2 and 3 is not a definitive statement of what is and what is not variable.

Table 2. Variability detections. t_{\max} is the maximum time span of observations: the minimum span was between 10 and 20 minutes. Two measures of variability amplitude are given: the average of the absolute relative magnitudes, $\overline{|m_d|}$, and the root-mean-square (RMS) of the relative magnitudes, σ_m . $\overline{\delta m_d}$ is the average photometric error in the light curve. $1 - p$ is the probability that the variability is intrinsic to the target. “Obs. run” gives the date (YY-MM) of the observations.

target	SpT	t_{\max} hours	$ m_d $ mags	σ_m mags	$\overline{\delta m_d}$ mags	p	No. of frames	No. of refs	Obs. run
2M0345	L0	53	0.012	0.017	0.011	4e-4	27	23	99-09
2M0913	L3	125	0.042	0.055	0.039	7e-4	36	14	99-01
2M1145	L1.5	124	0.026	0.031	0.022	1e-3	31	12	99-01
”	”	76	0.015	0.020	0.012	<1e-9	70	11	00-02
2M1146	L3	124	0.012	0.015	0.011	3e-3	29	7	99-01
2M1334	L1.5	126	0.017	0.020	0.011	<1e-9	51	12	00-02
SDSS 0539	L5	76	0.009	0.011	0.007	3e-5	31	24	00-02
SDSS 1203	L3	52	0.007	0.009	0.007	2e-3	51	13	00-02
Calar 3	M9	29	0.026	0.035	0.027	6e-4	42	21	99-01
S Ori 31	(M6.5)	50	0.010	0.012	0.007	4e-5	21	30	00-02
S Ori 33	(M6.5)	51	0.008	0.010	0.007	2e-3	21	43	00-02
S Ori 45	M8.5	50	0.051	0.072	0.032	5e-9	21	30	00-02

4.2 Comments on Individual Objects

Notes are now given on the light curves and power spectra of objects with statistically significant χ^2 detections. Brief comments are given at the end of the section on the non-detections. The implications of these results are discussed in section 5.

2M0345. The light curve shows no interesting features and there are no peaks in the cleaned power spectrum above four times the noise.

2M0913. This detection is due primarily to a significant drop in the flux around AJD 1187.5, going down to 0.13 magnitudes below the median for that night.

Table 3. Variability non-detections. The columns are the same as in Table 2 except that here $\overline{|m_d|}$ and σ_m are the upper detection limits on the variability amplitudes. The minimum time between observations of a given target was between 3 minutes (for 2M1439) and 35 minutes (for Roque 12).

target	SpT	t_{\max} hours	$\overline{ m_d }$ mags	σ_m mags	$\overline{\delta m_d}$ mags	p	No. of frames	No. of refs	Obs. run
2M0030	L2	51	0.018	0.025	0.020	0.21	37	27	99-09
2M0326	L3.5	49	0.021	0.029	0.017	0.56	19	36	99-09
2M1439	L1	97	0.007	0.009	0.007	0.10	48	13	00-02
Roque 11	M8	100	0.028	0.043	0.027	0.46	47	23	99-01
Roque 12	M7.5	50	0.016	0.022	0.015	0.02	17	43	99-09
Roque 16	M6	29	0.010	0.014	0.010	0.35	16	34	99-09
Teide 1	M8	100	0.029	0.041	0.030	0.10	47	23	99-01
S Ori 34	(M6)	51	0.008	0.010	0.007	0.28	21	43	00-02
S Ori 44	M6.5	51	0.030	0.035	0.026	0.06	21	30	00-02
S Ori 46	(M8.5)	51	0.032	0.041	0.030	0.03	21	43	00-02

There is no evidence for variability within the other three nights. There are no strong periodicities in the cleaned power spectrum, the strongest three being at 3.36 , 0.76 and 0.64 (± 0.08) hours, each at around only five times the noise level.

2M1145. Evidence for variability in this L dwarf was presented in [01], and it was tentatively claimed to be periodic with a period of 7.1 hours (using the Lomb–Scargle periodogram), pending confirmation. These data (and that for all other targets in [01]) have been re-reduced, and the new reduction still shows significant evidence for variability. However, the 7.1 hour periodicity is no longer significant in the cleaned power spectrum. Peaks are present at 5.4 ± 0.1 , 5.1 ± 0.1 , 1.47 ± 0.08 and 0.71 ± 0.08 hours, but are only marginally significant at around eight times the noise (Fig. 1). Note how difficult it would be to confidently identify these peaks in the dirty power spectrum.

The new reduction consists of an improved flat field, better fringe removal, more reference stars, and a few more points in the light curve. The light curves from the two reductions are consistent within their errors, but the power spectra differ, indicating that the 7.1 hour period was an artifact of higher noise and errors which crept into the first reduction.

2M1145 was re-observed at higher SNR and with more epochs in the 00-02 run. These data (Fig. 2) also show very strong evidence for variability, and the power spectrum shows significant peaks at the following periods (with power in units of the noise in parentheses): 11.2 ± 0.8 (31), 6.4 ± 0.3 (14), 2.78 ± 0.13 (7), 0.42 ± 0.13 (14) hours (Fig. 3). Note that the first period is four times the third, so these may not be independent. There are no common peaks in this power spectrum and the one from 99-01. This means that 2M1145 cannot have both stable surface features (over a one year timescale) and a rotation period of between 1 and 70 hours, as if it did we would have detected it in both runs (see section 5.1).

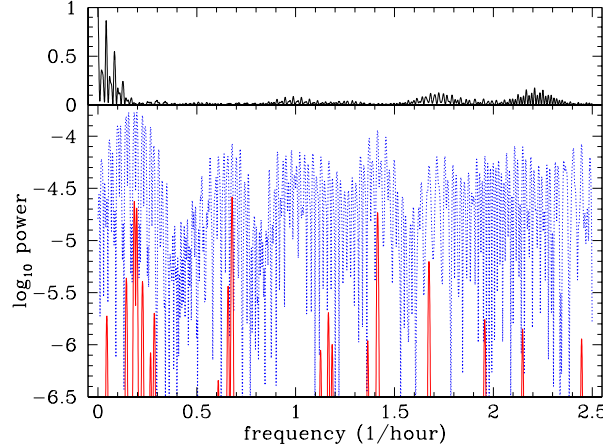


Fig. 1. Power spectrum for 2M1145 light curve from the 99-01 run. The bottom panel shows the dirty spectrum (dotted line) and the cleaned spectrum (solid line) in units of $\log_{10}(P)$. The noise level is at about $\log_{10}(P) = -5.6$. The top panel shows the shape of the spectral window function on a linear vertical scale, normalised to a peak value of 1.0.

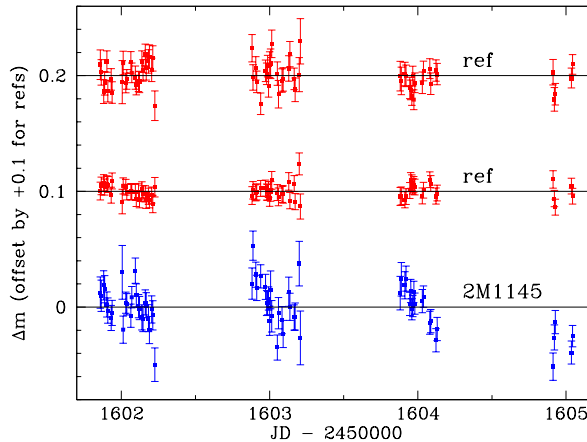


Fig. 2. Light curve for 2M1145 from the 00-02 run (bottom) plus a bright reference object (middle) and one of similar brightness to the target (top). The mean of these light curves each offset from the mean of the target star by the amount shown on the vertical axis. The mean for each light curve is shown as a solid line.

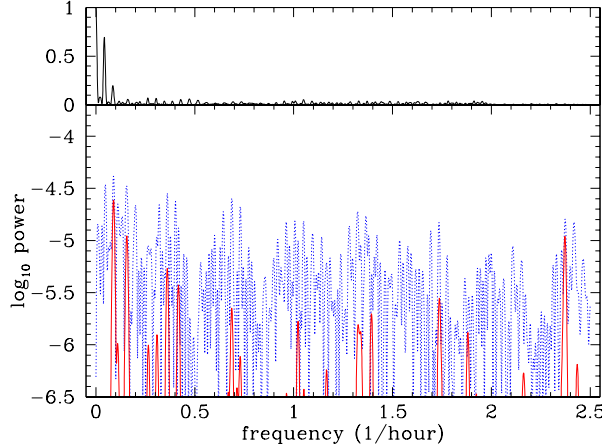


Fig. 3. Power spectrum for 2M1145 (from 00-02). The noise level is $\log_{10}(P) = -6.1$. See caption to Fig. 1.

2M1146. The power spectrum shows peaks at the following periods (with power in units of noise): 5.1 ± 0.1 (15), 3.00 ± 0.08 (6), 1.00 ± 0.08 (5), and 0.64 ± 0.08 (9) hours. The second and third are in the ratio 3:1, so are probably not independent. The one at three hours is more convincing based on the phase coverage in the phased light curve. This is one of only two L dwarfs in the sample which has a measured $v \sin i$, which, at 32.5 ± 2.5 km/s [04], implies a rotation period of 3.7 ± 0.3 hours, or less, due to the unknown inclination of the rotation axis (assuming a radius $0.1R_{\odot}$ [08]). 2M1146 appears to be an L dwarf–L dwarf binary [16] with a separation $0.3''$, as well as having a background early-type star only $1''$ away [14]. The light curve is a composite of variations in all three objects.

2M1334. This is significantly variable, and the light curve shows clear fluctuations within a number of nights (Fig. 4). The largest peak in the power spectrum (Fig. 5) is at 2.68 ± 0.13 hours at 12 times the noise.

Calar 3. The light curve shows no conspicuous features. The two most significant peaks in the power spectrum (at 14.0 and 8.5 hours) are less than five times the noise level, so are barely significant.

SDSS 0539. The seeing was worse than average for many of the frames in this field, so a larger photometry aperture of radius 5.0 pixels was used. (This increases the noise and hence lowers the sensitivity.) The significant χ^2 is partly due to the brighter points around AJD 1604. Otherwise the light curve shows no obvious patterns (see Fig. 6). The power spectrum shows a significant (20 times noise) peak at 13.3 ± 1.2 hours (Fig. 7). The light curve phased to this period is shown in Fig. 8.

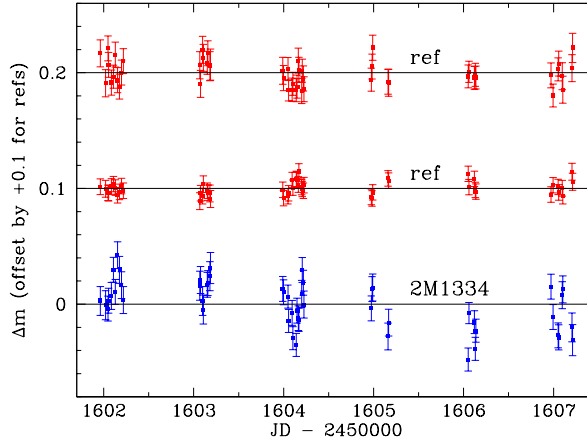


Fig. 4. Light curve for 2M1334 (bottom) plus a bright reference object (middle) and one of similar brightness to the target (top). See caption to Fig. 2.

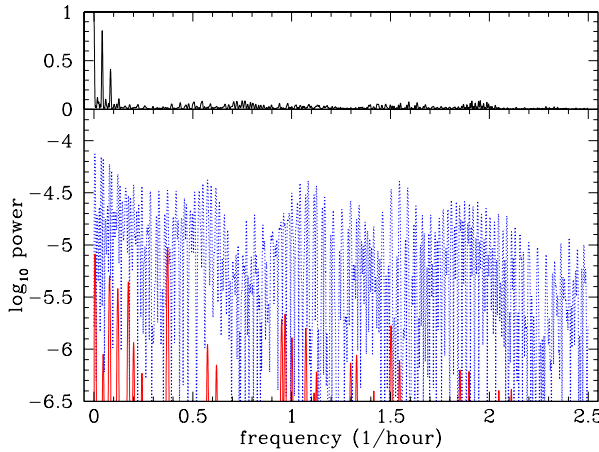


Fig. 5. Power spectrum for 2M1334. The noise level is $\log_{10}(P) = -6.2$. See caption to Fig. 1.

SDSS 1203. This variability is primarily due to a drop in brightness of about 0.02 magnitudes in four consecutive measurements around AJD=1606.1 (Fig. 9) lasting between one and two hours. This could be due to a short-lived surface feature, or possibly an eclipse by a physically associated companion.

S Ori 31. The power spectrum shows significant peaks at 7.5 ± 0.6 and 1.75 ± 0.13 hours at 18 and 9 times the noise level respectively. The former period dominates and may be the rotation period.

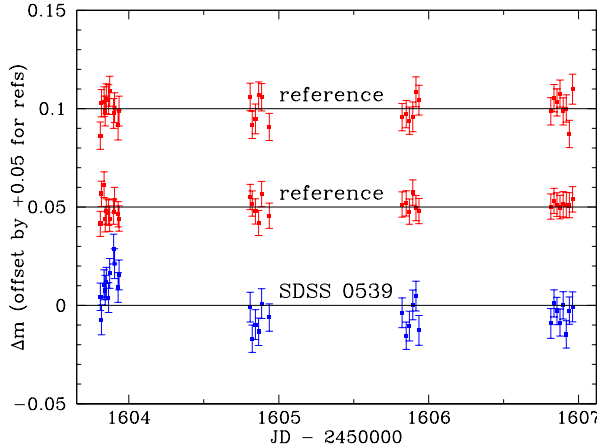


Fig. 6. Light curve for SDSS 0539 (bottom) plus a bright reference object (middle) and one of similar brightness to the target (top). See caption to Fig. 2.

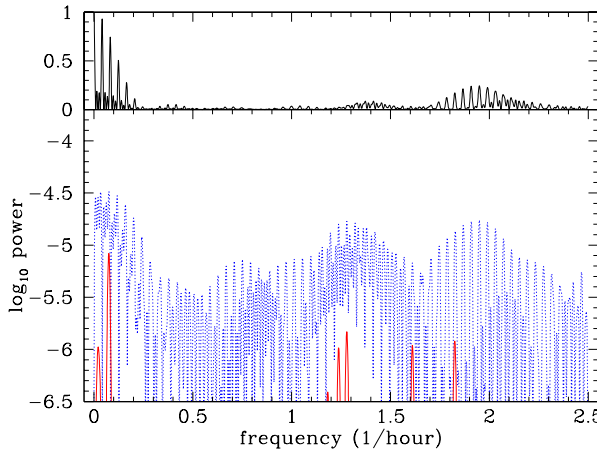


Fig. 7. Power spectrum for SDSS 0539. The noise level is $\log_{10}(P) = -6.4$. See caption to Fig. 1.

S Ori 33. The light curve shows a rise just before AJD 1606, and the power spectrum has peaks of 6 to 7 times the noise at 8.6 ± 0.7 and 6.5 ± 0.4 hours. The former has good phase coverage, so may be the rotation period, although it is not a strong peak.

S Ori 45. The light curve shows three points much lower than the average around AJD 1604.9, spanning a range of almost 0.25 magnitudes. There is, however, a bright ($\Delta m = 1.7$) nearby ($5''$) star which may well interfere with this variability determination. If these points are excluded there is no evidence for variability ($p = 0.18$). The most significant peak in the power spectrum is at 0.50 ± 0.13

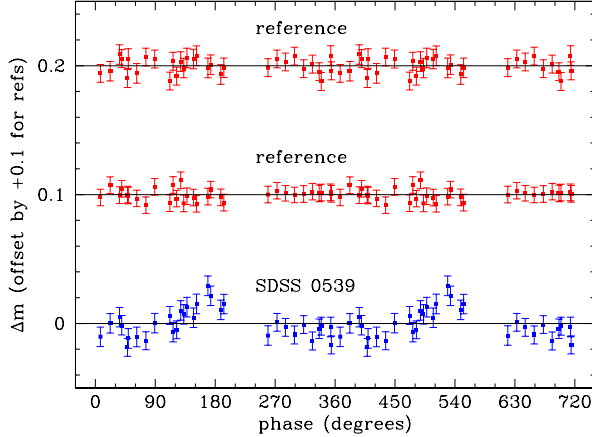


Fig. 8. Light curve (bottom) for SDSS 0539 phased to a period of 13.3 hours. The cycle is shown twice (${}^{\circ}-360^{\circ}$ and $360^{\circ}-720^{\circ}$). Also shown are two reference stars from Fig. 6 phased in the same way.

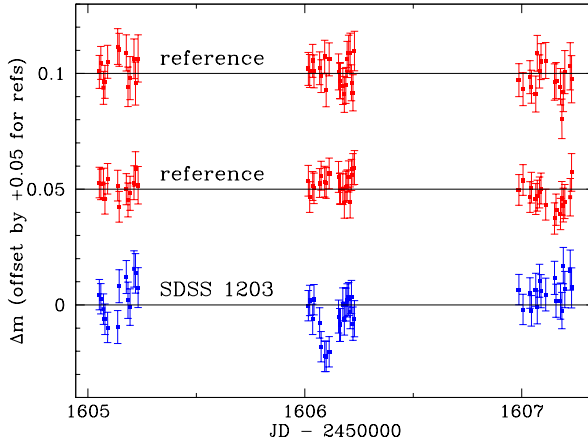


Fig. 9. Light curve for SDSS 1203 (bottom) plus a bright reference object (middle) and one of similar brightness to the target (top). See caption to Fig. 2.

hours (at 20 times the noise), which would be extremely fast if it is the rotation period.

Non-detections. 2M1439 has been measured to have a $v \sin i$ of 10 ± 2.5 km/s [04], implying a period of less than 12.1 hours for a $0.1R_{\odot}$ radius. S Ori 46 has a bright nearby star, which may affect the attempt to determine variability in this object. Roque 11 and Teide 1 have also been observed for variability in the I band by Terndrup et al. [28]. They also did not find evidence for variability, with measured values of σ_m of 0.041 and 0.045 magnitudes respectively.

4.3 Summary of the Results

11 of the 21 objects show evidence for variability at the 99% confidence level ($p = 0.01$). Of these, four (2M1145, 2M1334, SDSS 0539, S Ori 31) show strong evidence for variability ($p < 1e-4$). S Ori 45 is formally a fifth object with strong evidence for variability, but the presence of a bright close star makes us hesitant to draw this conclusion. In four cases (2M1146, 2M1334, SDSS 0539, S Ori 31) we have detected dominant significant periods in the range 3–13 hours, which may be rotation periods in all but the first case. S Ori 45 also has a dominant peak, but at 0.5 hours this would be very rapid if it is a rotation. The remaining objects do not show dominant periods, although the two earliest-type variables (S Ori 31 and S Ori 33) show near-sinusoidal light curves at detected periods. The light curve of one object, SDSS 1203, is essentially featureless except for a dip which may be due to an eclipse by a companion, although there is no direct evidence for this.

All of the objects which show variability have RMS amplitudes (σ_m in Table 2) between 0.01 and 0.055 magnitudes (ignoring S Ori 45), but most lie in the range 0.01 to 0.03 magnitudes and vary on timescales of a few hours. More detailed results are provided in Bailer-Jones & Mundt [02].

5 Discussion

5.1 Simulations of the Light Curves of Rotating Spotted Stars

The power spectrum is a representation of the light curve in the frequency domain. Specifically it gives the contributions to the variance in the light curve of sinusoids as a function of their frequencies. However, a significant peak in the power spectrum does not necessarily correspond to a *long-term* (and hence meaningful) periodicity. After all, *any* light curve – including a random one – can be described in terms of its power spectrum, as all features in the time domain must appear in the frequency domain somehow.

In particular, the “ideal” case of a pure sinusoidal light curve is only produced by a rotating star if one hemisphere is uniformly darker than the other and the star is observed along its equatorial plane. In contrast, a star with a single small surface feature (“spot”) would show a sinusoidal light curve only when the spot is on the observable hemisphere; for up to half of the rotation (depending on the inclination of the rotation axis) the light curve would be constant. A star with several spots will show a more complex behaviour, due to the variable number of spots observable (and hence modulating the light curve) at any one time. All of these variations will be explained by apparent “periods” in the power spectrum, some of which may even be significant relative to the noise.

We have carried out numerous simulations to understand the appearance of the light curve and its power spectrum due to such spots. Fig. 10 shows the light curve due to a single small dark spot on a star. If we rotate this star with a period of five hours and observe it with the same noise level and time sampling as one of the targets (2M1334), we obtain the power spectrum and phased light curve

in Fig. 11 and Fig. 10C respectively. The phased light curve is not sinusoidal, yet the power spectrum detects the rotation period.

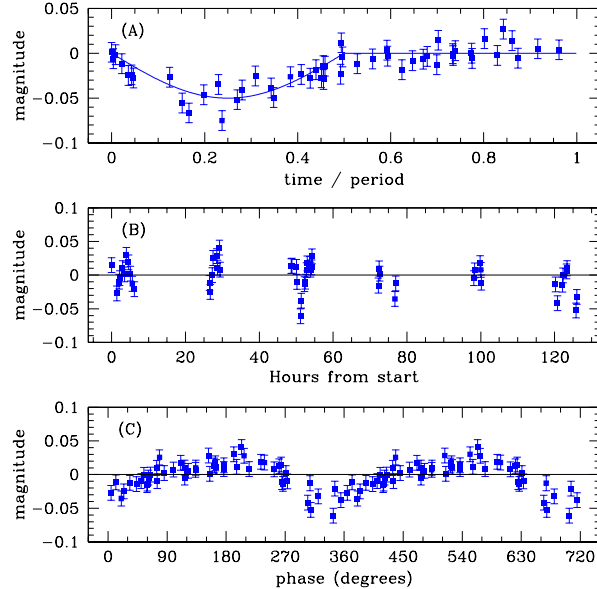


Fig. 10. (A) The solid line shows the true (noiseless) light curve of a rotating star viewed equatorially with a single dark spot of 0.05 magnitudes contrast. The star is rotated with a period of five hours and observed as 2M1334 was (i.e. with the same time sampling and with additive Gaussian noise of standard deviation 0.011 mags), giving the observed light curve in (B). (These points are also plotted in (A) wrapped to the rotation period.) Thus is significantly variable according to the χ^2 test ($p < 1\text{e-}9$). The cleaned power spectrum (Fig. 11) detects a period at 5.01 ± 0.10 hours: the light curve phased to this detected period *and phase* is shown in (C) (cycle shown twice).

Another simulation is shown in Fig. 12, which is due to a star with eight spots rotating with a period of ten hours. Here the contrast of the individual spots is much smaller, only -0.008 to $+0.014$ magnitudes. The sampling and noise from 2M1145 (00-02 run) is used and results in a significant variability detection according to the χ^2 test, but with $p = 0.005$ is close to the variable/non-variable cut-off. Despite this low SNR (and no detectable sinusoidal variation in Fig. 12C), the rotation period still clearly stands out in the cleaned power spectrum (Fig. 13).

We see that the light curve phased to the detected rotation period does not necessarily show sinusoidal (or even near-sinusoidal) variation. More extensive simulations with different numbers, amplitudes and phases of spots have been carried out. These indicate that even if the contrast of the spots (and hence the SNR) is very low, then provided the light curve shows significant variation according to the χ^2 test, the rotation period is seen at more than ten times

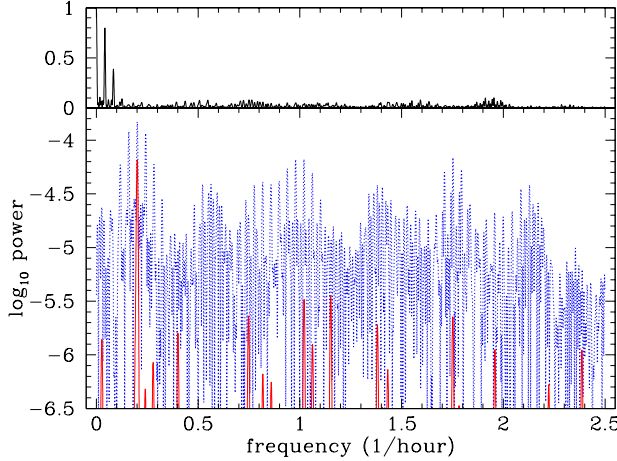


Fig. 11. Power spectrum for the simulated light curve shown in Fig. 10B. The noise level is $\log_{10}(P) = -6.2$. The same CLEAN parameters were used here as for the real data of section 4. See caption to Fig. 1.

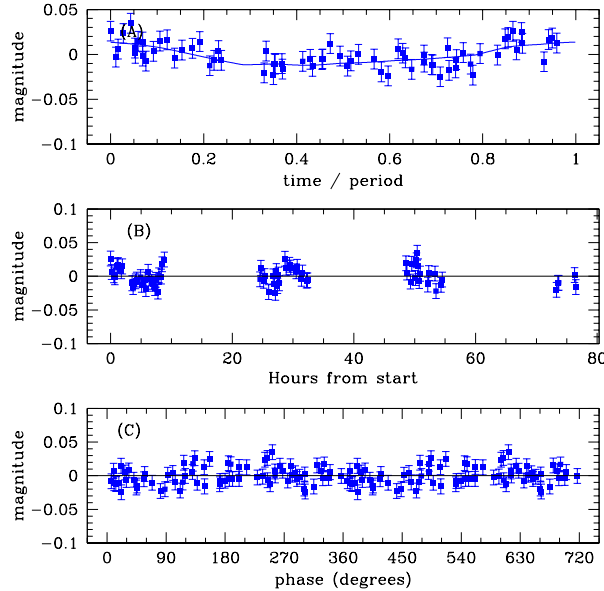


Fig. 12. Same as Fig. 10 except now for eight dark and bright spots with random phases. This gives a significant detection, although not overwhelming ($p = 0.005$), yet the cleaned power spectrum (Fig. 13) still detects the rotation period of 10 hours.

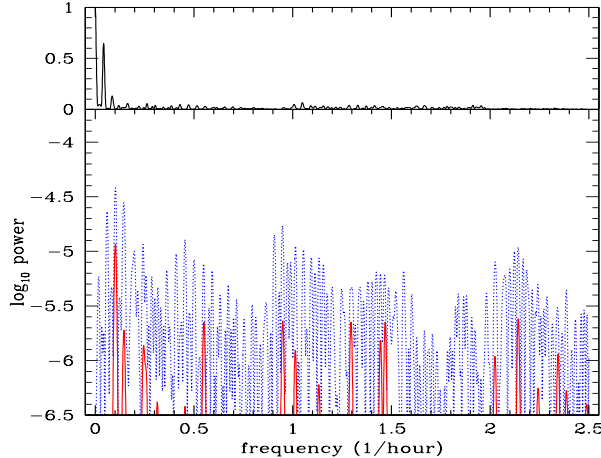


Fig. 13. Power spectrum for the simulated light curve shown in Fig. 12B. The noise level is $\log_{10}(P) = -6.1$. See caption to Fig. 1.

the noise in the power spectrum. Thus the absence of significant periods in the power spectrum for a variable light curve indicates *non-periodic* variations over the timescale of the observations.

5.2 Evidence for the Evolution of Surface Features

This non-periodic variability appears to imply one of three things:

1. the rotation period is shorter than the time span of observations;
2. the rotation period is longer than the time span of observations;
3. the surface features which are presumed to be modulating the light curve are not stable over the time span of observations.

The first of these implies a rotation period of less than 0.4 hours, which corresponds to an equatorial rotation speed of at least 240 km/s. Based on t_{\max} in Tables 2 and 3, the second possibility requires *maximum* $v \sin i$ values (i.e. when viewed equatorially) of between 1 and 4 km/s, assuming a radius of $0.1R_{\odot}$. These would be inconsistent with the measurements of Basri et al. [04], who report $v \sin i$ values between 10 and 60 km/s for 16 out of 17 late M and L field dwarfs. (According to models, even the youngest, warmest objects in Table 1 – those in σ Orionis – can have radii no larger than $0.2R_{\odot}$ [08], so $v \sin i$ could not be above 8 km/s for periods of order t_{\max} .) The results of Basri et al. therefore imply typical rotation periods of 1 to 10 hours, and the simulations have shown that such periods would have been detected in the light curves of the present sample, *if* these objects had stable modulating surface features. Yet some significantly variable objects show no significant periodicities. The logical explanation in these cases (especially 2M0345, 2M0913, 2M1145 and Calar 3) is, therefore, that these objects have surface features which evolve over the period of the observations, thus removing the rotational modulation from the light curve. For

2M1145 we possibly have more direct evidence of this, as the two light curves from one year apart show no common periods.

5.3 Physical Nature of the Surface Features

Magnetically-induced star spots are common in solar-type stars, the magnetic field being produced by the $\alpha\Omega$ dynamo. This appears not to operate in low mass stars and brown dwarfs, yet a turbulent dynamo may [08]. However, recent observations imply that chromospheric activity – and, perhaps, the contrast of magnetic spots – decreases rapidly between spectral types M7 and L1 [03][12]. In comparison, Fig. 14 shows the amplitude of variability (or upper limit thereon) as a function of spectral type for the sample in this paper. Whereas 7/10 of objects later than M9 show variability, only 2/9 earlier than this do. (The average detection limits/amplitudes are almost identical in the two regions, so this is not an artifact.) If the variability were due to magnetic spots, then in the light of the activity decline we would expect variability to be *less* common among later-type objects, not *more* common as seen here. Although this could also be an age effect (all of the targets of type M9 and earlier are cluster members with ages less than 120 Myr) it hints towards a non-magnetic origin of the surface features.

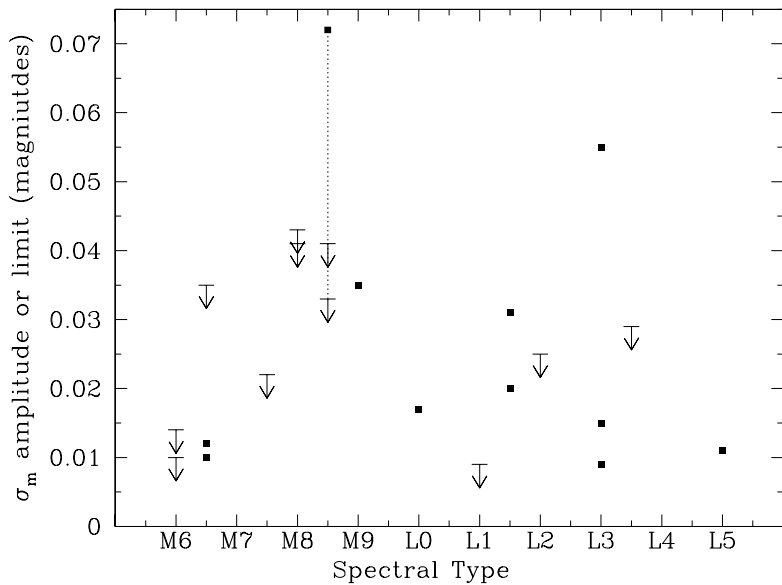


Fig. 14. Relationship between variability amplitudes (squares) or upper limits to variability (arrows) and spectral type. S Ori 45 (M8.5) is plotted as both an amplitude and a limit (connected with a dotted line) depending on whether the first night of data is included or not. The plot using $|m_d|$ rather than σ_m as the amplitude measure is very similar.

Another candidate for producing variability is photospheric dust clouds. Modelling of optical and infrared spectra show that solid particles form in late M and L dwarfs [07][09][12][19]. While we may expect this dust to gravitationally settle below the photosphere, certain processes (such as turbulence) may prevent this, and models which include dust opacity (as well as removing dust constituents from the equation of state) give better fits to the near infrared spectra of ultra cool dwarfs [09]. This dust could form into large-scale opaque clouds. Their evolution over a few rotation periods could account for the variability reported in this paper, possibly driven by rapid rotation and turbulence. The clouds would have to be relatively large, as many small clouds evolving independently would have an insignificant net effect on the light curve. As more dust can form in cooler objects, we may expect more variability in later-type objects, as seen in Fig. 14. However, given the small amount of data on any one object, it is premature to attempt to determine the characteristics or dynamics of the variability patterns.

Other causes of the variability can be considered, including flaring, accretion (for the youngest objects) or infall in an interacting binary. However, these all rely on transient phenomena, so no one explanation for all objects is that satisfactory.

6 Summary

Light curves for 21 late M and L dwarfs were obtained to probe variability on timescales between a fraction of an hour and over 100 hours. 11 objects showed evidence for variability at the 99% confidence level according to a χ^2 test, with amplitudes between 0.009 and 0.055 magnitudes (RMS). The ten non-detections have upper limits on their RMS amplitudes of between 0.009 and 0.043 magnitudes.

Power spectral analysis showed that a few objects (2M1146, 2M1334, SDSS 0539, S Ori 31) had significant, dominant periods between 3 and 13 hours. For 2M1334, SDSS 0529 and S Ori 31 these may be the rotation periods. The remaining seven significantly variable light curves did not show dominant periods, and in at least three cases (2M0345, 2M0913, Calar 3) there are not even any significant periods. Simulations showed that any plausible period would have been detected for these objects. It was concluded that this non-periodic behaviour is probably due to the evolution of surface features (assumed to produce the variability) on timescales of a few to a few tens of hours. These variabilities blur the rotation period, inhibiting its detection. This is supported by observations of 2M1145 one year apart, in which the two light curves have no common periodicities.

It was speculated that this variability (at least for the later-type objects) is due to photospheric dust clouds, the evolution of which could be driven by turbulence and rapid rotation. In support of this is the greater propensity for variability in objects later than M9, while magnetic activity (which could otherwise support the presence of magnetically-induced spots) declines greatly beyond M7.

Acknowledgements

The author would like to thank Harry Lehto for use of his CLEAN code and advice on its use. The data in this paper were obtained with the 2.2m telescope at the German–Spanish Astronomical Center at Calar Alto in Spain.

References

01. C.A.L. Bailer-Jones, R. Mundt: *A&A* 348, 800 (1999)
02. C.A.L. Bailer-Jones, R. Mundt: *A&A* submitted (2000)
03. G. Basri, Cool Stars 11 (ASP Conf. Ser.), in press (2000)
04. G. Basri, S. Mohanty, F. Allard, et al.: *ApJ* 538, 363 (2000)
05. V.J.S. Béjar, M.R. Zapatero Osorio, R. Rebolo: *ApJ* 521, 671 (1999)
06. A.J. Burgasser, J.D. Kirkpatrick, M.E. Brown, et al.: *AJ* 120, 1100 (2000)
07. A. Burrows, C.M. Sharp: *ApJ* 512, 843 (1999)
08. G. Chabrier, I. Baraffe: *ARA&A*, in press (2000)
09. G. Chabrier, I. Baraffe, F. Allard, P. Hauschildt: *ApJ* 542, 464 (2000)
10. T.J. Deeming: *Astrophysics & Space Science* 36, 137 (1975)
11. X. Fan, G.R. Knapp, M.R. Strauss, et al.: *AJ* 119, 928 (2000)
12. J.E. Gizis, D.G. Monet, I.N. Reid, J.D. Kirkpatrick, J. Liebert, R.J. Williams: *AJ* 120, 1085 (2000)
12. H.R.A. Jones, T. Tsuji: *ApJ* 480, L39 (1997)
14. J.D. Kirkpatrick, I.N. Reid, J. Liebert, et al.: *ApJ* 519, 802 (1999)
15. J.D. Kirkpatrick, I.N. Reid, J. Liebert, et al., *AJ* 120, 447 (2000)
16. D.W. Koerner, J.D. Kirkpatrick, M.W. McElwain, N.R. Bonaventura: *ApJ* 526, L25 (1999)
17. S.L. Leggett, T.R. Geballe, X. Fan, et al.: *ApJ* 536, L45 (2000)
18. H.J. Lehto: private communication (2000)
19. K. Lodders: *ApJ* 519, 793 (1999)
20. E.L. Martín, G. Basri, M.R. Zapatero-Osorio, R. Rebolo, R.J. García López: *ApJ* 507, 41 (1998)
21. E.L. Martín, X. Delfosse, G. Basri, B. Goldman, T. Forveille, M.R. Zapatero-Osorio: *ApJ* 118, 2466 (1999)
22. T. Nakajima, T. Tsuji, T. Maihara, et al.: *PASJ* 52, 87 (2000)
23. K.S. Noll, T.R. Geballe, S.K. Leggett, M.S. Marley: *ApJ* 541, L75 (2000)
24. R. Rebolo, M.R. Zapatero Osorio, E.L. Martín: *Nature* 377, 129 (1995)
25. I.N. Reid, J.D. Kirkpatrick, J.E. Gizis, et al.: *AJ* 119, 369 (2000)
26. R. Rebolo, E.L. Martín, G. Basri, G.W. Marcy, M.R. Zapatero-Osorio: *ApJ* 469, L53 (1996)
27. D.H. Roberts, J. Léhar, J.W. Dreher: *AJ* 93, 968 (1987)
28. D.M. Terndrup, A. Krishnamurthi, M.H. Pinsonneault, J.R. Stauffer: *ApJ* 118, 1814 (1999)
29. C.G. Tinney, A.J. Tolley: *MNRAS* 304, 119 (1999)
30. M.R. Zapatero Osorio, R. Rebolo, E.L. Martín, et al.: *A&AS* 134, 537 (1999)